Experimental study of dispersion and miscible viscous fingering of initially circular samples in Hele-Shaw cells

R. Maes,[1] G. Rousseaux,[2] B. Scheid,[3] M. Mishra,[1,4] P. Colinet,[3] and A. De Wit[1]
[1]*Nonlinear Physical Chemistry Unit and Center for Nonlinear Phenomena and Complex Systems, Université Libre de Bruxelles (ULB), CP 231, Boulevard du Triomphe, 1050 Brussels, Belgium*
[2]*Laboratoire J.-A. Dieudonné, Université de Nice-Sophia Antipolis, UMR CNRS-UNS 6621, Parc Valrose, 06108 Nice Cedex 02, France*
[3]*Laboratory TIPs (Transfers, Interfaces and Processes) - Fluid Physics Unit and Center for Nonlinear Phenomena and Complex Systems, Université Libre de Bruxelles (ULB), CP 165/67, 50 av. F.D. Roosevelt, 1050 Brussels, Belgium*
[4]*Department of Mathematics, Indian Institute of Technology Ropar, 140001 Rupnagar, India*

(Received 23 December 2009; accepted 29 November 2010; published online 22 December 2010)

Experimental studies are conducted to analyze dispersion and miscible viscous fingering of initially circular samples of a given solution displaced linearly at constant speed U by another solution in horizontal Hele-Shaw cells (two glass plates separated by a thin gap). In the stable case of a dyed water sample having the same viscosity as that of displacing nondyed water, we analyze the transition between dispersive and advective transport of the passive scalar displaced linearly. At low displacement speed and after a certain time, the length of the sample increases as a square root of time allowing to compute the value of a dispersion coefficient. At larger injection speed, the displacement remains advective for the duration of the experiment, with a length of the sample increasing linearly in time. A parametric study allows to gain insight into the switch from one regime to another as a function of the gap width of the cell. In the unstable case of viscous glycerol samples displaced by dyed water, the rear interface of the sample where less viscous water pushes more viscous glycerol is unstable with regard to viscous fingering. The interface deforms into fingers, the number and size of which depend on the viscosity ratio between the two solutions and on the displacement speed. We study the influence of these viscous fingering phenomena on the increased spreading of the sample for various mobility ratios and injection speeds.
 [doi:10.1063/1.3528039]

I. INTRODUCTION

Characterizing the spreading of an initially localized sample of a given solute displaced linearly by a flow in a porous medium is a challenging problem from a fundamental point of view and also in numerous fields of application. In the case of groundwater contamination by a given pollutant,[1–3] it is of interest to be able to predict for instance the widening of the pollution zone in time when the initial spatial extension of the spill is finite due to a contamination localized in space/time. If the contaminant is displaced underground by a carrier fluid of same viscosity, dispersion can increase the spreading of the sample in space/time.[4] Solute dispersion refers to the spreading of an initially localized sample of a given solute due to the combination of molecular diffusion and flow velocity gradients.[5–10] This spreading can even be worse if the sample has a different viscosity than the displacing fluid, in which case viscous fingering (VF) phenomena can take place. Viscous fingering is a hydrodynamic instability that occurs when a fluid of given viscosity μ_1 displaces a more viscous fluid of viscosity $\mu_2 > \mu_1$ in a porous medium:[11] the interface between the two fluids is unstable and "finger-like" patterns grow in the course of time. In the case of finite samples of a more viscous fluid surrounded and displaced by a less viscous miscible one, VF contributes to widen the sample and increases the spreading in comparison with the hydrodynamically stable situation.[2,3,12] In this context, understanding the contributions of dispersion and of VF to the spreading characteristics is crucial for water resources management.[3,12–14]

Another application where understanding such spreading is important can be found in liquid chromatography, which consists of displacing samples through porous media in order to separate their chemical components. Dispersion of the sample in a chromatographic column influences the broadening of the concentration peaks and thus the efficiency of the separation.[15,16] If, moreover, the sample viscosity is different from the viscosity of the displacing fluid, VF can also distort and widen the concentration peaks (see Refs. 3 and 17–26 and references therein). Here, again, forecasting the effect of those two contributions on the extent and the shape of the concentration peaks is of crucial importance.

Several theoretical works have contributed to quantify the influence of viscous fingering on the widening of finite size samples.[3,17–21,27,28] From an experimental point of view, studies of dispersion and fingering in porous media have been made in the case of variable-density and/or variable-viscosity flows using glass beads with index of refraction matching that of the displacing fluid in three-dimensional tanks,[22,23] beads in Hele-Shaw cells, or NMR imaging techniques.[24,25,29–31] Unfortunately, those techniques imply no direct experimental visualization of the full dynamics.

Some works have favorably used simple Hele-Shaw cells without beads as an experimental model for bidimensional porous media.[32–39] The main advantage of this setup is to allow simultaneous visualization and quantification of the concentration field evolution without disturbing the flow field.[12,13] The reason for considering the Hele-Shaw cell as a bidimensional porous medium[11] is the fact that the averaged flow speed across the cell thickness can be described by Darcy's law if the gap width is thin enough as compared to the characteristic length of the dynamics under investigation. More precisely, if $\bar{U}$ and L are typical velocity and length scales of the experiment, while b is the gap width and ν the kinematic viscosity, the typical viscous time scale b^2/ν has to be much smaller than the convective time scale $L/\bar{U}$ for this approximation to hold.

In this context, the objective of this work is to analyze experimentally the influence of dispersion and viscous fingering on the spreading of initially circular samples displaced linearly in a Hele-Shaw cell. In particular, our goal is to quantify the contribution of these phenomena to the spatial spreading of the samples.

To study the effect of viscous fingering, we need first to understand the transport process in the cell without VF. For homogeneous fluids, the transport is described by the dispersion tensor derived by Aris[6] to generalize Taylor's results[5] to the transport of a nonreactive solute between two plates. In single-phase systems with unidirectional flow, and assuming that the characteristic diffusion time scale $\tau_{\text{diff}}=b^2/D_m$ (D_m is the molecular diffusion coefficient) is much smaller than the convective time scale $\tau_c=L/\bar{U}$, Aris showed that the variation of the concentration field $C(x,t)$ averaged across the gap follows a one-dimensional advection-diffusion equation, i.e.,

$$\frac{\partial C}{\partial t}+\bar{U}\frac{\partial C}{\partial x}=D\frac{\partial^2 C}{\partial x^2}, \tag{1}$$

where $\bar{U}$ is the average flow velocity. The longitudinal dispersion coefficient D can be written as[6,8,10]

$$D=D_m+K\frac{b^2\bar{U}^2}{D_m}, \tag{2}$$

where $K=1/210$. Previous experimental results focusing on dispersion in a Hele-Shaw cell considered the case of a denser fluid sinking into another one in a vertical cell.[12,13] In this case, it has been shown that the variation of densities between the two fluids influences the dispersion process. To minimize buoyancy effects and concentrate on viscous fingering, we consider here the case of a horizontal cell.

To obtain both stable and viscously unstable situations, we displace finite size liquid samples by another liquid of same or lower viscosity within a Hele-Shaw cell. The samples are, at any time, totally surrounded by the displacing liquid and we follow their distortion optically. We measure the longitudinal extent, perimeter, and surface of the sample in time for various displacement speeds, gap width of the cell, and mobility ratios to demonstrate enhanced spreading due to fingering.

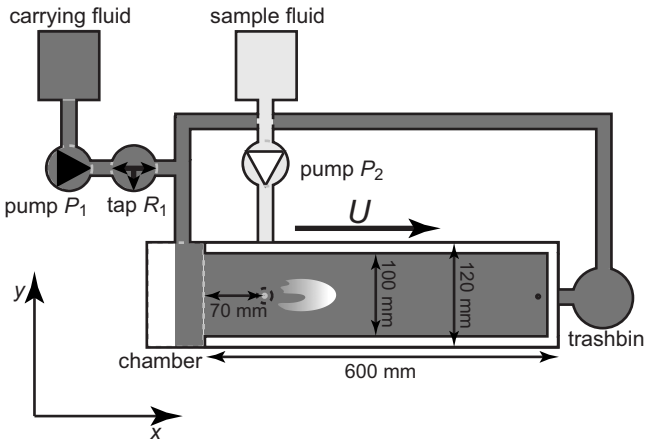

FIG. 1. Schematic view of the Hele-Shaw cell.

The article is therefore organized as follows. We first describe the experimental setup in Sec. II. We discuss the dispersion effects in the Hele-Shaw cell in Sec. III and then describe the effect of viscous fingering in Sec. IV. Conclusion is given in Sec. V.

II. EXPERIMENTAL SETUP

Our experimental setup (see Fig. 1) is a Hele-Shaw cell consisting of two transparent glass plates of length $L_x=600$ mm, width $L_y=120$ mm, and thickness $L_z=13$ mm oriented horizontally in the gravity field above a lightening table and below a CCD (charge-coupled device) camera. The plates are separated by a gap of thickness b controlled by the use of "U-shaped" spacers cut out of 0.25 or 0.5 mm thick mylar sheets. The spacer branches of 10 mm width put on the sides of the plates lead to an available channel of 100 mm width. The plates are inserted into a metallic structure. The waterproofness of the system is ensured by using a range of screws that push a metal ruler placed on a rubber joint at the edges of the upper plate.

As in Ref. 38, we inject the displacing fluid through an injection valve consisting of a rectangular aperture through which fluids can be injected linearly at one lateral side of the cell at constant speed $U=\frac{3}{2}\bar{U}$ (note that U will refer to the maximal velocity at midheight of the gap, while $\bar{U}$ is the averaged velocity). The circular sample is injected through a 1 mm hole drilled in the lower glass plate and centered at 70 mm downstream the linear injection valve. The fluids are evacuated through a 1 mm large hole sink centered at the opposite end of the cell. The volume of the sample injected in the cell is controlled by using a peristaltic pump (P_2 in Fig. 1), with a precision of 10^{-3} mm^3. The speed U of the linear displacement is fixed by using a gear pump (P_1), which controls the injection speed of the displacing fluid with a precision of 10^{-2} mm/s.

For each experiment, we first filled the cell with the displacing fluid. When the cell was completely filled, we stopped the linear injection and waited until this fluid was at rest. We then injected radially a fixed volume of sample through the injection hole using the pump P_2. When this injection was finished, we disconnected the pump P_2 from

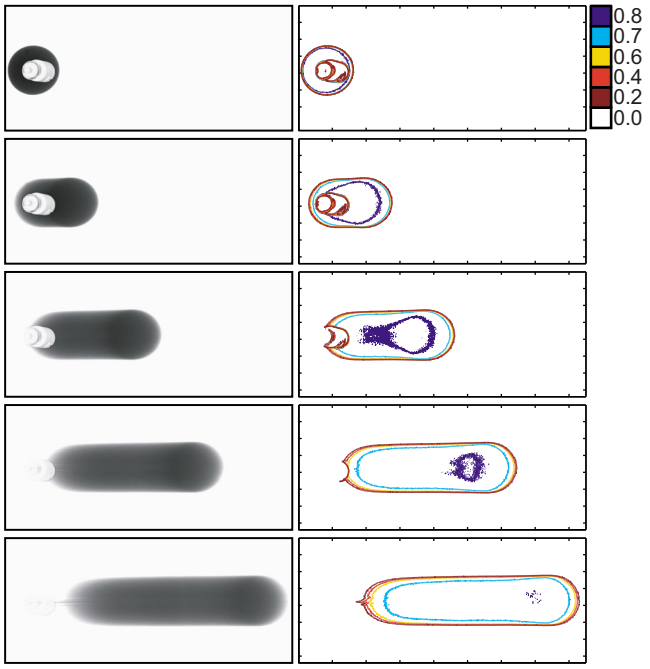

FIG. 2. (Color online) Temporal evolution of the sample (left) and corresponding isoconcentration curves (right). The injection speed is 2.5 mm/s and the time between each frame is 40 s. The white spot in the center of the initial sample is the injection valve.

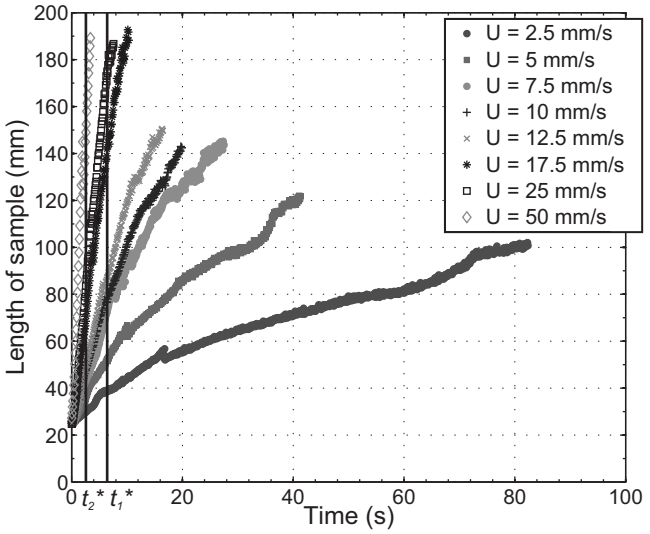

FIG. 3. Length of sample as a function of time for various injection speeds U from $U=2.5$ mm/s (lowest curve) to $U=50$ mm/s (top left curve). Estimates t_1^* and t_2^* of the transition between advective and dispersive regimes are defined in Sec. III C.

the system. We then injected the other fluid through the cell from a lateral side at a constant speed U controlled by the pump P_1 (linear injection).

In the stable case (no viscosity contrast), the displacing fluid is nondyed water and the samples are composed of water colored by amaranth red. At small concentration, this dye does not affect the density or viscosity of the mixture, yet it allows to visualize the sample transport into the cell.[39] In the unstable case, the displacing fluid is dyed water and the initially circular sample is a nondyed more viscous water-glycerol mixture. The proportion of glycerol in the sample determines its viscosity. Experiments are performed at room temperature.

We followed the dynamics in the system using a CCD camera connected to a computer-driven imaging system acquiring a gray level photograph every 0.2 s with an image resolution of 1280×1024 pixels. In order to get accurate results, we applied a post-treatment to each picture using a MATLAB code. We first aligned all the pictures using a bilinear interpolation algorithm, then cropped the zone of interest and substracted a background picture taken before each experimental run. Finally, we renormalized the gray levels to see the maximum value of the dye as 1 and the minimum value as 0.

III. STUDY OF THE DISPERSION IN THE CELL

Figure 2 shows a typical stable displacement of the colored water sample by a linear injection of nondyed water at constant speed U from left to right. The shape of the sample, initially circular, becomes elongated with displacement. To follow the dynamics into more details, we compute the isoconcentration curves (see Fig. 2, right panel) for the following gray levels: 0, 0.2, 0.4, 0.6, 0.7, and 0.8. The level 0.2 corresponds here to the outer dark surface of the sample. Using this representation, it can be seen that the dynamics inside the sample is strongly asymmetric. As the sample spreads in time, the concentration at the center of the sample decreases, as shown by the disappearance of the 0.8 isoconcentration level. Simultaneously, the higher concentration zone (>0.6) is drifted toward the front of the sample, where it is wider than at the back.

A. Transition between dispersive and advective regimes

To determine whether the stable displacement inside the cell follows a dispersive or an advective regime, we measured the temporal evolution of the length of the sample. To do so, we counted on each horizontal line of the digitalized image the number of gray pixels. We then defined the length of the sample as the length of the longest line. The temporal changes of this length are shown in Fig. 3 for a 0.123 ml sample (or 25 mm initial length) displaced in the cell at various flow velocities U, the gap width being fixed at $b=0.25$ mm. Note that on all curves, a small sudden and abrupt decrease in the length is observed when the sample disengages from the shadow of the sample injection mechanism. We have checked that this has a negligible influence on our quantitative results.

It is observed that at high speed ($U=17.5,25,50$ mm/s), the length of the sample increases linearly with time, the slope of the line being approximately equal to the (maximal) axial velocity of the flow. This suggests that advection is in these cases the dominant transport phenomenon. At lower speed (here typically for $U=2.5,5,7.5$ mm/s), the length of the sample tends to evolve as a square root of time, suggesting a dispersive regime. Indeed, writing Eq. (1) in the frame moving with the mean velocity of the flow, we get

TABLE I. Parameters of experiments (stable case): injection speed U, estimated dispersion coefficient D, estimated molecular diffusion coefficient D_m, agreement between the measured length evolution in time and a dispersive behavior (r_1) or an advective behavior (r_2), characteristic convective time $\tau_c=\ell_0/U$ with $\ell_0=25$ mm, and corresponding Péclet number (defined in the text).

U (mm/s)	D (mm^2/s)	D_m (10^{-3} mm^2/s)	r_1^2	r_2^2	$\tau_c=\ell_0/U$ (s)	Pe
2.5	1.34	0.5	0.95	0.87	10	0.23
5.0	4.5	0.6	0.96	0.89	5	0.45
7.5	11.4	0.6	0.97	0.89	3.3	0.68
10.0	14.5	0.8	0.96	0.94	2.5	0.90
12.5	—	—	0.94	0.97	2.0	1.13
17.5	—	—	0.90	0.99	1.4	1.61
25.0	—	—	0.89	0.99	1.0	2.26
50.0	—	—	0.89	0.98	0.5	4.52

$$\frac{\partial C}{\partial t}=D\frac{\partial^2 C}{\partial x^2}. \tag{3}$$

For the initial condition $C(x)=1$, where $-\ell/2\leq x\leq+\ell/2$ and $C(x)=0$ elsewhere, the well-known analytical solution of this equation can be written as a superposition of two error functions,[40] which actually approaches a Gaussian shape at sufficiently large times. Formally, the concentration profile therefore extends to infinity as soon as $t>0$. However, experimentally the concentration cannot be measured below $(1.5\pm0.4)\%$ of its initial value. If we cut the theoretical concentration profiles obtained at several successive times on our experimental time scales (typically $0<t<100$ s) at the 1.5% level, we get that $(\ell_x-\ell_0)^2$ evolves linearly in time, where ℓ_x is the length of an evolving sample of initial length ℓ_0. We determine the angular coefficient by a fit to obtain that

$$(\ell_x-\ell_0)^2\approx 37.7Dt, \tag{4}$$

which allows to estimate the dispersion coefficient D from the experimental data.

For quantitative measurements, we fit $(\ell_x-\ell_0)^2$ as extracted from the data using the least-squares method with two curves: a linear trend line (dispersive case) and a square function (advective case). When the coefficient of determination r_2^2 of the square function is larger than r_1^2, the one of the linear trend, the regime is assumed to be advective (results are shown in Table I). We find that for velocities lower than $U=12.5$ mm/s, the dynamics is globally better described by dispersion. Figure 4 shows the estimated value of the dispersion coefficient for flow velocities up to $U=10$ mm/s. For each of these dispersion coefficients, we compute D_m, the molecular diffusion coefficient, using Eq. (2). Performing an average over the values obtained for each velocity and taking into account the error resulting from the fit and the uncertainty on the detection level, we find that the diffusion coefficient is $D_m=(0.7\pm0.5)\times10^{-3}$ mm^2/s. We draw the theoretical value of dispersion coefficients D for $D_m=0.7\times10^{-3}$ mm^2/s as a function of speed U in Fig. 4. The values of D for $U=2.5,5,7.5$ mm/s are well predicted by the theoretical curve given by Eq. (2). For $U=10$ mm/s, D is not well aligned on this curve. This could be explained by the fact that it takes some time to reach the Taylor–Aris regime and we performed the estimation of D using all the data points shown in Fig. 3. This can be further understood if we compare the characteristic diffusion time scale $\tau_{\text{diff}}=b^2/(4\pi^2D_m)=2.26$ s (here estimated taking into account the factor $4\pi^2$ resulting from the resolution of the diffusion equation for the slowest symmetric mode) with $b=0.25$ mm and $D_m=0.7\times10^{-3}$ mm^2/s to the convective time scale $\tau_c=\ell_0/U$ (see Table I) constructed here using a typical initial length $\ell_0=25$ mm of the sample to be advected. The corresponding Péclet number $\text{Pe}=\tau_{\text{diff}}/\tau_c$ computed in Table I shows that the dispersive regime holds in the cases where Pe is smaller or of the order of one. Despite this good agreement, it must be noted that the choice of the length scale ℓ_0 used in the definition of the convective time scale τ_c is somehow arbitrary (see also Sec. III C) and hence there remains some uncertainty in the value of Pe. To quantify in details the transition between advective and dispersive regimes would rather require solving the full three-dimensional advection-diffusion problem (numerically, most likely). However, this remains outside the scope of the present work.

Figure 5 shows the evolution of the square of the calculated length variation of the sample using $D_m=0.7\times10^{-3}$ mm^2/s compared to the experimental data. For $U=5.0$ and 7.5 mm/s, we see that the curves initially look like a parabola. This can be explained by the fact that the Taylor–Aris regime is not yet reached for such short times.

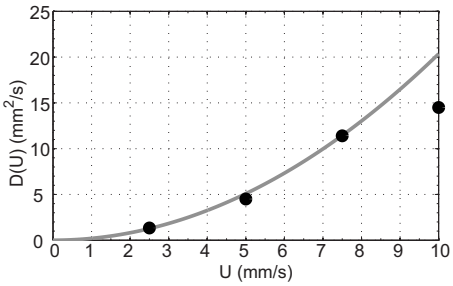

FIG. 4. Dispersion coefficient as a function of speed for flow velocities lower than $U=12.5$ mm/s for gap width $b=0.25$ mm (points) and theoretical curve corresponding to Eq. (2) and $D_m=0.7\times10^{-3}$ mm^2/s (line).

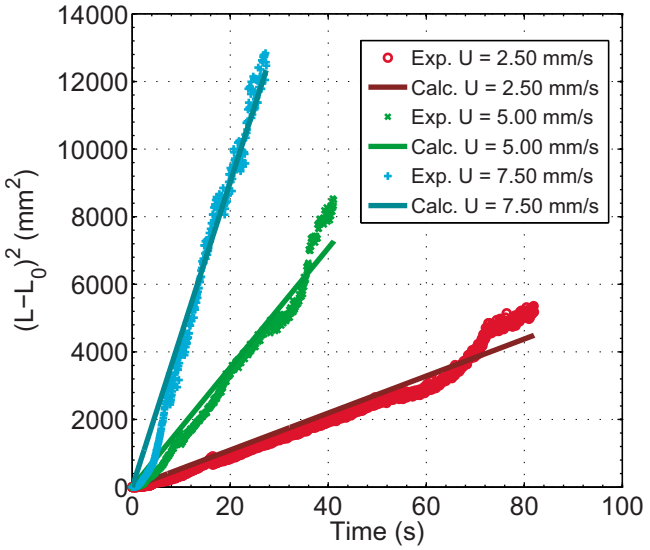

FIG. 5. (Color online) Comparison of calculated and measured length of samples for $U=2.5,5,7.5$ mm/s from bottom to top.

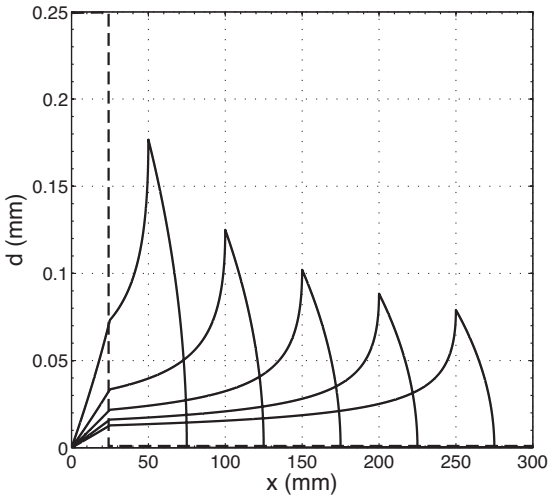

FIG. 7. Temporal evolution of the thickness of the colored layer along the longitudinal direction x of the cell (for a gap width $b=0.25$ mm) in the case of a sample of 0.123 ml (corresponding to an initial width $\ell_0=25$ mm) displaced with a linear injection speed $U=50$ mm/s. The profiles shown are calculated every second. The dashed line corresponds to the initial sample.

B. Advective regime

To gain quantitative insight into our experimental data for larger U, let us analyze the advection of a passive tracer (or dye) by a Poiseuille flow within the gap width of a one-dimensional Hele-Shaw cell.[41] We consider a rectangular sample of initial length ℓ_0 and height b as sketched in Fig. 6. We assume that there is a Poiseuille flow deforming the sample in the Hele-Shaw cell gap and for which the velocity profile has the form

$$v(z) = U\left(1 - 4\frac{z^2}{b^2}\right). \tag{5}$$

In order to know what concentration distribution is measured from a top view, we compute the thickness $d(x,t)$ of the colored layer crossed by the light in each point along the x axis as a function of time, assuming that the dye is advected without any diffusion.

The axial coordinate of the extremum of the Poiseuille parabola for the back interface is $x_{m,1}(t)=Ut$, while for the front interface it is $x_{m,2}(t)=Ut+\ell_0$. Note that $x_{m,2}$ thus corresponds to the theoretical length of the sample (see Fig. 6). We define three zones along the x axis, as shown in Fig. 6:

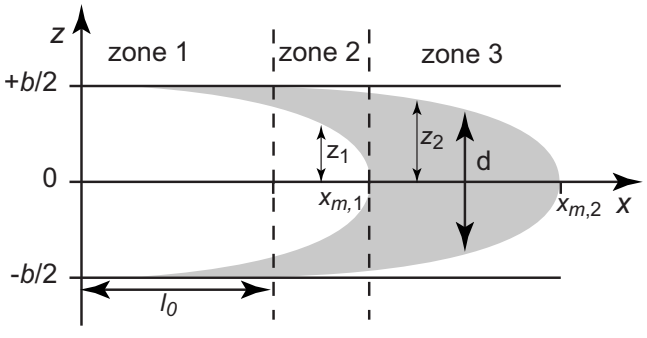

FIG. 6. Two-dimensional model for Poiseuille flow in the gap of the cell.

(a) zone 1: $0 \le x \le \ell_0$,
(b) zone 2: $\ell_0 < x \le x_{m,1}(t)$,
(c) zone 3: $x_{m,1}(t) < x < x_{m,2}(t)$.

As the flow is along x, the axial displacement of a fluid element with a fixed coordinate $\tilde{z}$ is given by $x(\tilde{z},t) = x(\tilde{z},0)+v(\tilde{z})t$. Thus, using Eq. (5), the height of the colored zone at each axial location x can be expressed as

$$d(x,t) = \begin{cases} b - 2\tilde{z}_1(x,t) & \text{in zone 1} \\ 2[\tilde{z}_2(x,t) - \tilde{z}_1(x,t)] & \text{in zone 2} \\ 2\tilde{z}_2(x,t) & \text{in zone 3,} \end{cases} \tag{6}$$

where $\tilde{z}_1$ is defined as

$$\tilde{z}_1(x,t) = \frac{b}{2}\sqrt{1 - \frac{x}{Ut}}$$

(thickness between the rear interface of the deformed sample and $z=0$) and $\tilde{z}_2$ is defined as

$$\tilde{z}_2(x,t) = \frac{b}{2}\sqrt{1 - \frac{x-\ell_0}{Ut}}$$

(thickness between the frontal interface and the centerline $z=0$).

This allows to plot the thickness of the colored layer as a function of x at different times. The results are the profiles shown in Fig. 7 for a 0.123 ml sample displaced with a linear injection speed of 50 mm/s.

To take into account the experimental resolution in concentration, we cut the profiles below a thickness d_c of colored water corresponding to 1.5% of the gap width, i.e., $d_c=3,75$ μm. The calculated sample length becomes in this case $\ell_a \simeq (1-2d_c/b)Ut+\ell_0$ (clearly, ℓ_a reduces to $x_{m,2}$ when $d_c=0$). Nevertheless, this "cutting" correction being very small in the expression for ℓ_a, we have chosen to plot in Fig. 8 the lengths of the sample as given by $x_{m,2}$, i.e., for $d_c=0$. We see that for $U=17.5,25,50$ mm/s, the agreement is

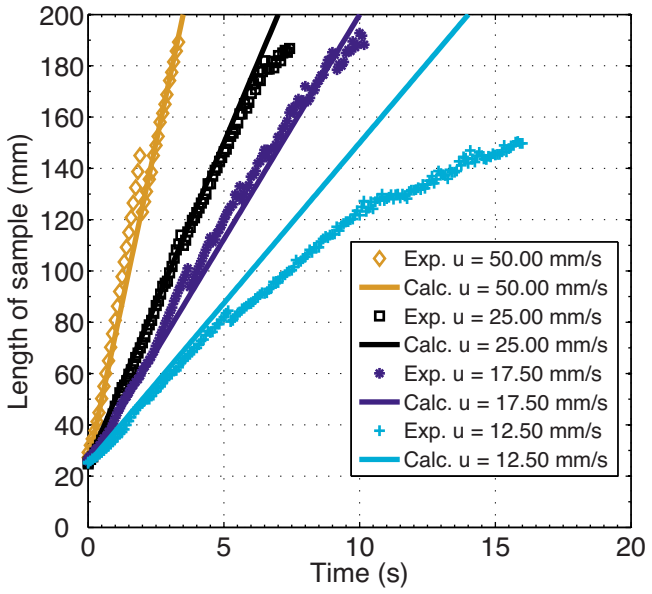

FIG. 8. (Color online) Comparison of calculated and measured length of samples for $U=12.5, 17.5, 25, 50$ mm/s from bottom to top.

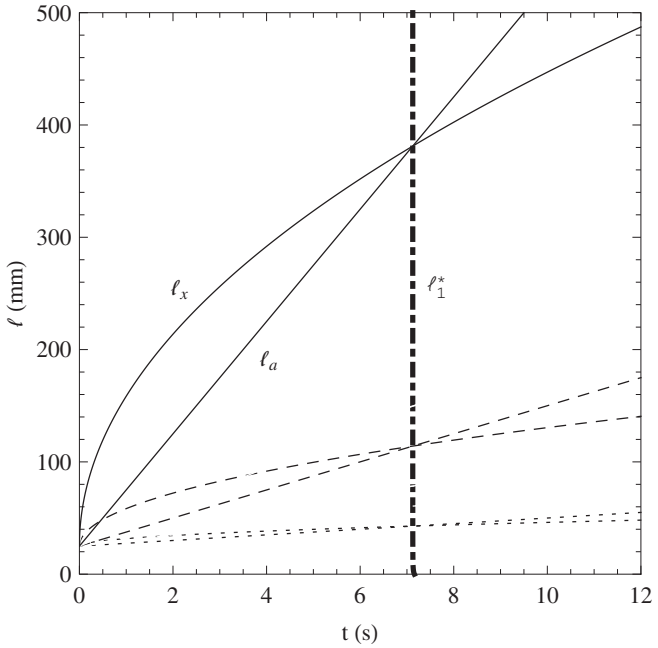

FIG. 9. First estimate of the sample length ℓ_1^* (dot-dashed line) corresponding to the transition between the pure advective regime (ℓ_a) and the pure dispersive regime (ℓ_x) for three different speeds: 2.5 mm/s (dotted lines), 12.5 mm/s (dashed lines), and 50 mm/s (solid lines).

rather satisfactory. In contrast, the evolution of the length of a sample displaced at $U=12.5$ mm/s does not fit with the evolution of the length calculated following this advective two-dimensional model. This indicates the influence of dispersion for speeds around and smaller than 12.5 mm/s on our experimental time scales.

C. Transition length and time between dispersive and advective regimes

Having determined in Sections A and B the sample lengths for the pure dispersive regime (ℓ_x) and for the pure advective regime (ℓ_a), we can *a priori* estimate the length $\ell_1^* \equiv \ell_x = \ell_a$ at which the two are equal, i.e.,

$$\ell_1^* \equiv \ell_0 + \sqrt{aDt} = \ell_0 + Ut, \tag{7}$$

where $a=37.7$, as determined in Eq. (4). This indeed provides a first estimate of the cross-over between the two regimes, as seen in Fig. 9. On the other hand, as mentioned in Sec. III A, a purely dispersive regime is expected when the Taylor–Aris criterion $b^2/4\pi^2 D_m \ll \ell^*/U$ is satisfied. Assuming that the length to be used in this criterion is the advective length ℓ_0+Ut (which is likely to be valid for the initial stage), we get a second estimate of the cross-over between both regimes as

$$\ell_2^* \equiv \frac{b^2 U}{4\pi^2 D_m} = \ell_0 + Ut. \tag{8}$$

The corresponding transition time for each estimate, using Eq. (2) for D, has the form

$$t_1^* = \frac{4aKb^2}{9D_m} + \frac{aD_m}{U^2} \quad \text{and} \quad t_2^* = \frac{b^2}{4\pi^2 D_m} - \frac{\ell_0}{U}. \tag{9}$$

Furthermore, for sufficiently large speed U (as is the case for the range of speeds considered in this paper), these estimates can be simplified to

$$t_1^* \approx \frac{4aKb^2}{9D_m} \quad \text{and} \quad t_2^* \approx \frac{b^2}{4\pi^2 D_m}. \tag{10}$$

Notice that in this limit, t_2^* reduces simply to the diffusion time scale τ_{diff}, while t_1^* reduces to $3\tau_{\text{diff}}$, approximately. The diffusive nature of the transition time indicates that the system is dominated by advection for $t<t^*$ and by Taylor–Aris dispersion for $t>t^*$.

In the present case, we get $t_1^* \approx 7.1$ s ($t_2^* \approx 2.3$ s) for $b=0.25$ mm and $t_1^* \approx 28.5$ s ($t_2^* \approx 9$ s) for $b=0.50$ mm (see next section). Both results seem to agree, at least qualitatively, with our experimental results (see Figs. 3 and 10). However, the uncertainty on the molecular diffusion coeffi-

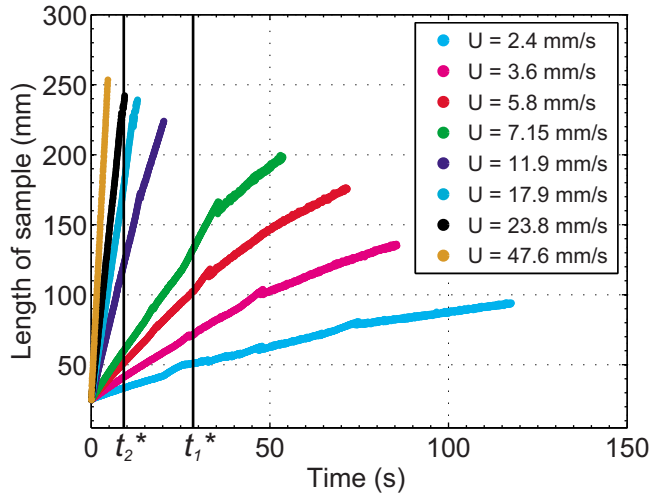

FIG. 10. (Color online) Same as for Fig. 3 with $b=0.50$ mm.

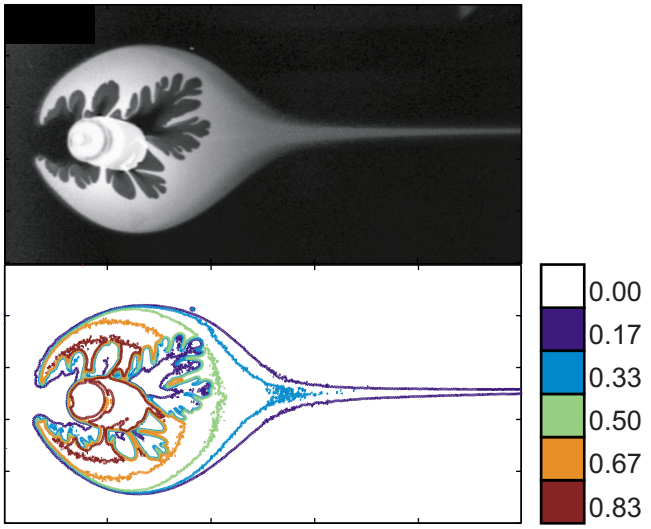

FIG. 11. (Color online) Fingering of a sample of glycerol displaced by dyed water for a mobility ratio $R=2.03$ and an injection speed $U=12.50$ mm/s. The cropped zone is 66 mm large and 130 mm long. The gap width $b=0.25$ mm. The top figure is the direct image recorded by the camera at $t=12$ s and the lower one shows the computed isoconcentration curves.

cient does not allow to discriminate between t_1^* and t_2^*, and further investigations would be necessary to possibly define the transition time more accurately.

D. Influence of the gap width

A similar series of experiments as those shown in Fig. 3 has been performed for a larger gap width, here $b=0.50$ mm. Not surprisingly, we found that dispersive regimes are only observed on our experimental time scales for really low speeds (Fig. 10). As expected for dispersion in a given gap width, it takes more time for molecular diffusion to homogenize the distortion of the sample by the Poiseuille flow in larger gap widths. Hence, for a given speed, the dispersive regime is established at larger times in thicker cells (in agreement with estimates of the previous section).

IV. VISCOUS FINGERING

Let us now consider the linear displacement of initially circular samples of glycerol by water. Unlike in the previous discussion, the sample of glycerol being displaced is now undyed while the displacing water is dyed in order to more clearly demonstrate the viscous fingering of the water into the glycerol (Fig. 11).

A. Fingering dynamics

As the glycerol sample is more viscous than the displacing water, i.e., as the mobility ratio, $R=\log(\mu_2/\mu_1)>1$ (where μ_1 is the viscosity of the displacing fluid and μ_2 the viscosity of the sample), the dynamics is quite different than in the equal viscosity situation. First of all, as seen in Fig. 11 for instance, the overall shape of the sample quickly changes to a drop-like form with a spindle that eventually connects the sample to the sink hole located at the other end of the cell. As the displacing dyed water is less viscous than the uncolored sample, viscous fingering occurs at the rear side of the sample. As anticipated from classical knowledge of previous VF studies,[11,42] the situation is more unstable for larger mobility ratios and high injection speeds. This is featured here by the fact that fingering appears faster and with a smaller wavelength when the mobility ratio R, or the speed U, is increased.

Figure 12 shows the temporal evolution of the system for three different injection speeds at a given mobility ratio $R=1.03$. At low speed [Fig. 12(a)], the deformation of the rear interface is affected by the injection hole which imprints a deformation into a large blob. At intermediate velocity, the injection hole still affects the deformation but fingers with a smaller wavelength developed within the central blob. At larger injection speeds, VF is strong enough to develop numerous thin and long fingers that invade the viscous sample through the rear interface.

The influence of the viscosity ratio at a fixed speed of 40 mm/s is shown in Fig. 13. The sample is displaced much slower in the cell in the case of large mobility ratios than for small mobility ratios. For instance, comparing Figs. 13(a) and 13(c), we see that for the same time, the sample has moved away from its injection point in the low mobility ratio case, while it seems almost stationary in the high mobility ratio case. We also note that at a small mobility ratio $R=1.03$ [Fig. 13(a)], thin fingers appear later when the sample has already been displaced beyond the injection hole. At $R=1.55$, long and thin fingers develop on the rear interface when the sample is still above the injection hole [Fig. 13(b)]. At an even larger $R=2.03$, thicker fingers that undergo repeated tip splittings are obtained right away [Fig. 13(c)]. So, in general, the complexity of the viscous fingering pattern increases with the mobility ratio. Eventually, in very destabilizing conditions, i.e., $R=2.49$, situations can also be observed where the less viscous fluid is so much more mobile than the sample fluid that it forms a channel into the middle of the sample and directly goes to the sink expelling the more viscous fluid on the sides of the cell (Fig. 14). As a side remark, note that such a leftover of the more viscous phase outside the path of the flow is particularly detrimental for oil recovery or pollution events for instance.

B. Quantitative analysis

Our objective is to quantify the influence of this viscous fingering on the spreading of the sample. To obtain quantitative data, we followed the temporal evolution of isoconcentration curves. To do so, we extracted from the CCD images isoconcentration levels (which enclose the zones of the picture where the gray level normalized between 0 and 1 is superior or equal to a certain threshold), as seen in Fig. 15. Those levels are chosen here as equal to 0, 0.17, 0.33, 0.50, 0.67, and 0.83. The level 0.83 is determined experimentally to be the upper level allowing to fully cover the sample without displaying significant noise. An interval of 0.17 between the various plotted isoconcentration contours was determined to be sufficient to clearly describe the dynamics and isolate each isoconcentration curve from the others.

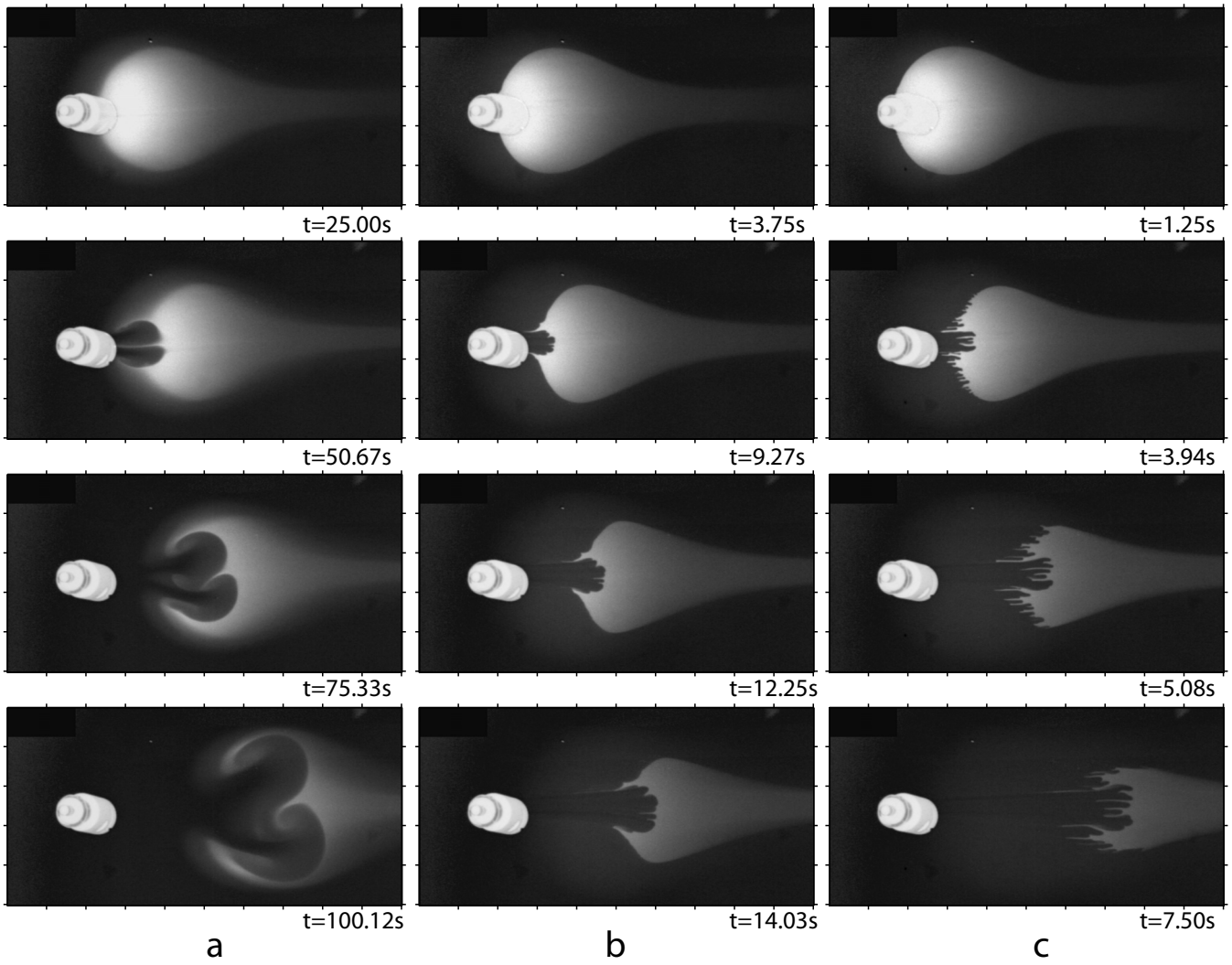

FIG. 12. Viscous fingering of glycerol samples displaced by dyed water: three different experiments with the same mobility ratio $R=1.03$ shown at various times for three different displacing speeds: (a) $U=2.5$ mm/s, (b) $U=12.5$ mm/s, and (c) $U=25$ mm/s. The gap width $b=0.25$ mm and the field of view 95 mm $\times$ 186 mm.

We then measured the temporal evolution of the perimeter and the area of the isoconcentration levels for various values of R and U.

C. Effect of the flow velocity

As shown in Fig. 12, by increasing the injection speed U for a given mobility ratio R, we observe the appearance of more and thinner fingers. We also see that the number of tip-splitting events increases with speed. We plot the corresponding perimeter of the isoconcentration curve corresponding to a gray level larger than 0.83 as a function of time in Fig. 16. We observe at the beginning a very slow increase of this perimeter due to the deformation of the sample as in stable cases before the fingering instability sets in. An abrupt increase occurs once fingering starts. The larger U, the earlier this increase starts. After a while, a decrease appears corresponding to the time when the sample starts to exit the cell. At low speed ($U=5.00$ mm/s), the perimeter increases slowly because of the slow development of one or two large fingers which finally merge [as shown in Fig. 12(a)]. At larger speed ($U=30$ mm/s), this perimeter growth has a much larger slope before the sample is quickly washed out of the cell which corresponds to a decrease of the perimeter after its maximum.

Surprisingly, a nonmonotonous change with speed of the maximum amplitude of the perimeter is observed: indeed, this maximum is smallest for intermediate values of U. In particular, for $U=10$ mm/s, the maximum value of the perimeter in the course of time is the smallest value measured here. Actually, the speed $U=10$ mm/s corresponds to a transition between a regime at $U<10$ mm/s characterized by the development of a few large fingers which finally collapse to a regime at larger U, in which numerous fingers invade the sample and split a few times before the sample leaves the cell. For velocities larger than $U=10$ mm/s, the increase of the maximum value of the perimeter is associated to the increase of the number of fingers and of tip-splitting phenomena in time.

Figure 17 shows the evolution of the area within the isoconcentration curve corresponding to a gray level superior to 0.83 for $R=1.03$. The overall decrease of the area in time is due to the fact that the sample is drained out of the cell

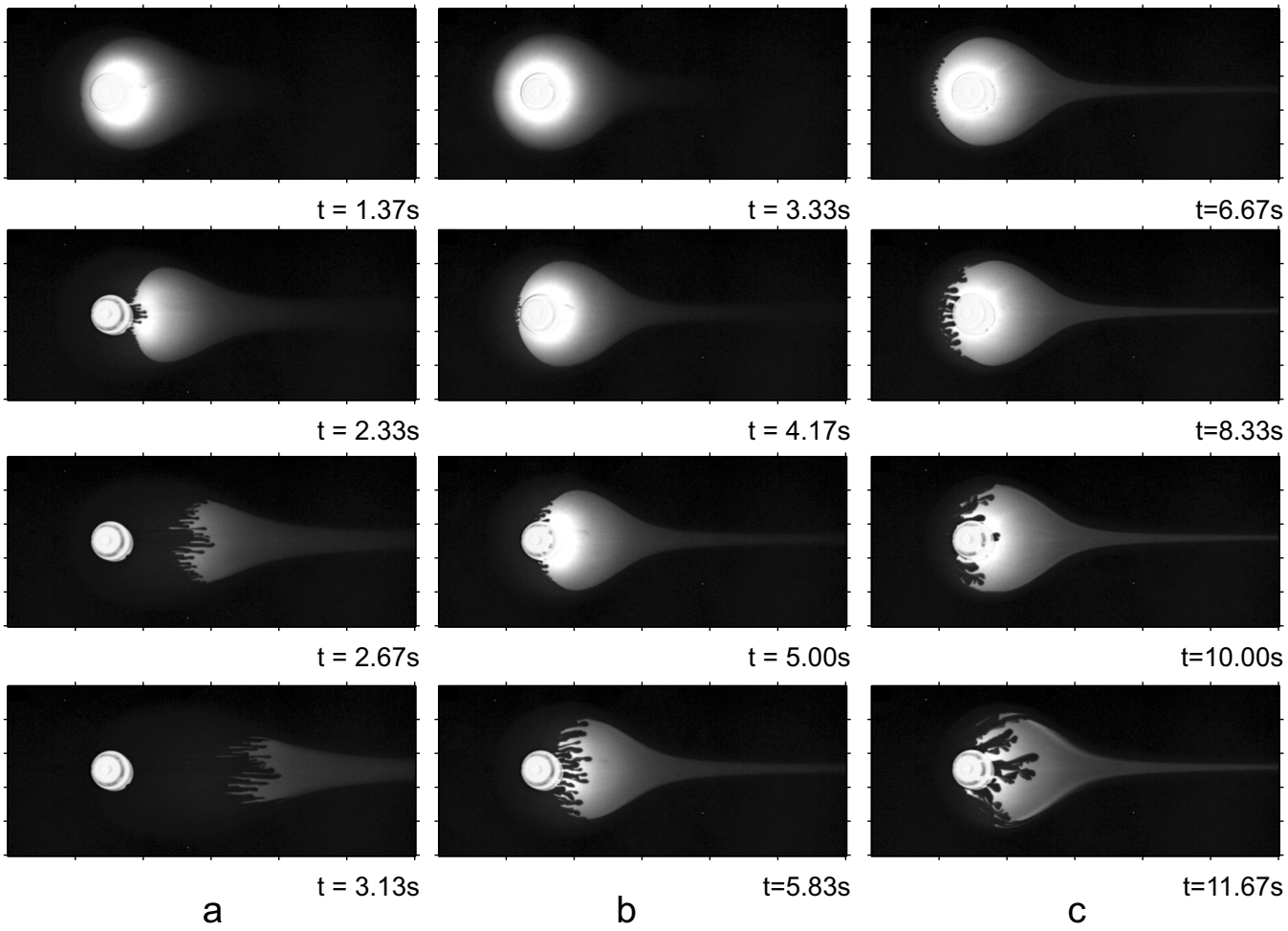

FIG. 13. Viscous fingering of glycerol samples displaced by dyed water: three different experiments with the same injection speed $U=40.00$ mm/s shown at various times for different mobility ratios: (a) $R=1.03$, (b) $R=1.55$, and (c) $R=2.03$. The gap width $b=0.25$ mm and the field of view 100 mm$\times$240 mm.

through the sink. This is in contrast to the stable case ($R=0$) for which the area grows before reaching the sink (Fig. 2). For the unstable case, the larger U, the faster the expel of the sample out of the cell and the smaller the area for a given time. This feature, which is due to the specific choice of initially circular samples and of a point sink, does not allow to appreciate the influence of fingering on increase of area as much as in the case of rectangular samples and a sink line as done in numerical simulations.[3,19,20] However, fingering still increases the total area as it leads to the appearance of a local bump in the temporal evolution of the area. This bump corresponds to the development of the fingers. As for the perimeter, the maximum value of the area reached by this bump does not vary monotonically: for this mobility ratio, the transition between the regime characterized by the development of a few large fingers (e.g., $U=5$ mm/s) and the regime characterized by strong tip-splitting processes (e.g., $U=12.5$ mm/s) is also to be found around $U=10$ mm/s. We also see that the bump is lower in high speed cases. As we can see in Fig. 12, it is indeed observed that for high speeds, the sample shows lower spreading in the transverse direction to the flow.

D. Effect of the mobility ratio

The temporal evolution of the area of samples of different viscosities displaced at a same velocity is shown in Fig. 18. As the mobility ratio increases from 1.03 to 2.49, the sample stays longer in the cell and the fingering is more important, which implies a later drop to zero (corresponding to the total expulsion of the sample out of the cell) and a wider bump due to fingering in the curve. When a "channel" of water is formed through really viscous glycerol samples (as in Fig. 14 for $R=2.49$), fingering is not well developed which implies a lower bump, but remains of the sample are found in the cell for really longer times than for less viscous case. For instance, at speeds lower than $U=7.5$ mm/s, it takes more than ten times longer to evacuate the whole sample for $R=2.49$ than for $R=1.03$.

The evolution of the perimeter of the sample for a fixed velocity and five different mobility ratios is shown in Fig. 19. The stable case $R=0$ shows a moderate increase of the perimeter before a sudden drop which is due to the sample flowing out of the cell on really short time scales. When fingering takes place, i.e., when $R>0$, the distortion of the sample implies an increase of the perimeter, followed by a

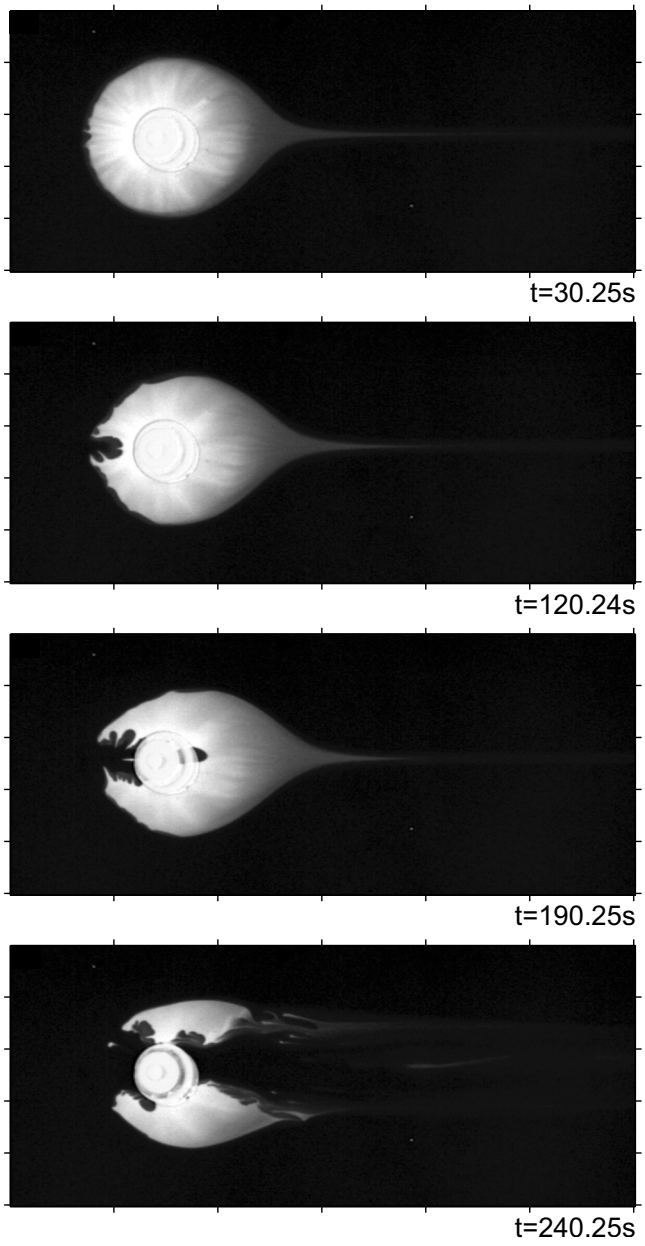

FIG. 14. Viscous fingering for high mobility ratio $R=2.49$. Displacing fluid is injected at speed $U=7.50$ mm/s. The gap width $b=0.25$ mm and the field of view 100 mm $\times$ 240 mm.

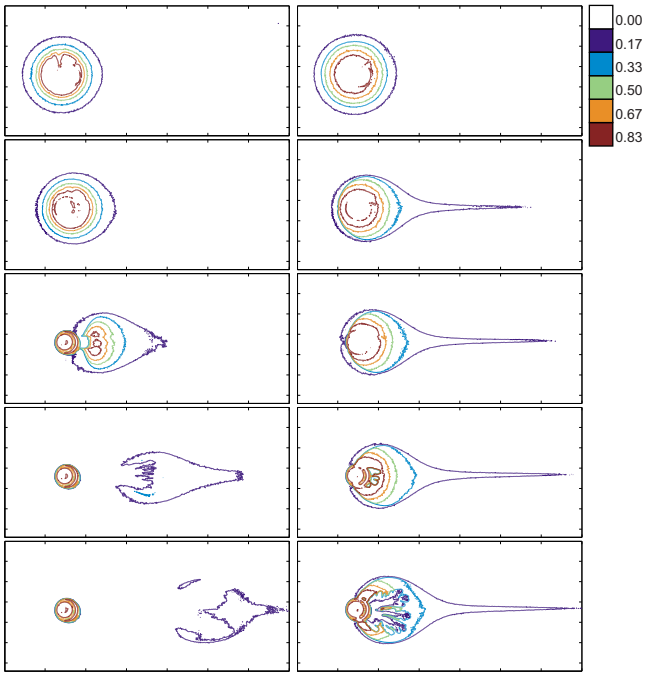

FIG. 15. (Color online) Temporal evolution of isoconcentration curves at fixed speed $U=7.50$ mm/s and different mobility ratios for cases $R=1.03$ (left) and $R=2.03$ (right). The time between each frame is 9.00 s.

decrease when the sample reaches the sink. For $R=1.03$ and for the low speed used here ($U=7.5$ mm/s), the sample is flowing out of the cell before the onset of significant fingering, which implies only a moderate increase of the perimeter before the latter decreases. The maximal value of the perimeter clearly increases at larger R. However, for really viscous samples, in the case $R=2.49$, the formation of the channel described above implies that the perimeter does not reach very large values. It should also be noticed that viscous fingering then still takes place in the remains of the sample, which explains the second bump in the curve after the first peak. On the applications side, this result indicates that for instance, the extent of the contamination zone for highly viscous contaminants in real porous media could be lower than in the case of contaminants of moderate viscosity, although it will take more time to wash those highly viscous contaminants out of the porous medium.

V. CONCLUSION

When finite size samples of a given fluid are displaced by another miscible fluid in a porous medium or like here in a model Hele-Shaw cell, their spreading depends crucially on whether the interface between the two fluids is stable or not with regard to fingering phenomena. For a stable sample of

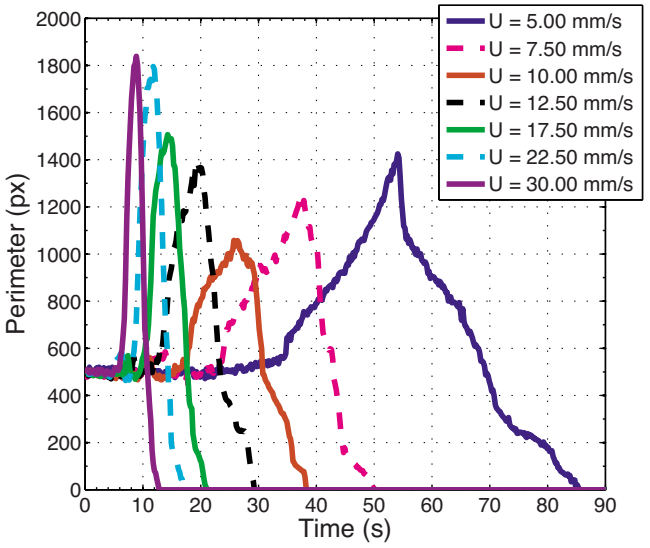

FIG. 16. (Color online) Temporal evolution of the perimeter for seven different injection speeds for a fixed mobility ratio $R=1.03$ for $U=5$ mm/s (rightmost curve) to $U=30$ mm/s (leftmost one).

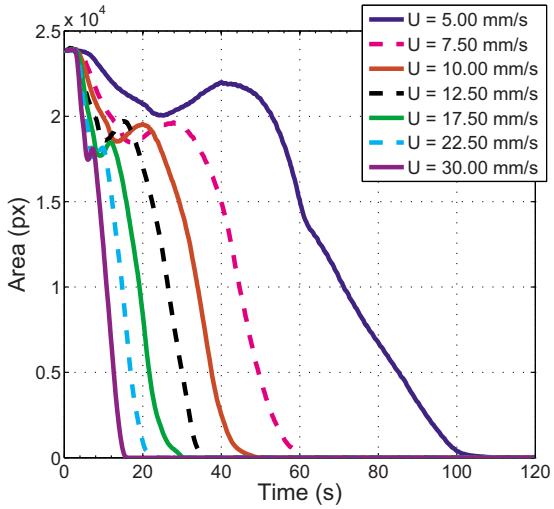

FIG. 17. (Color online) Temporal evolution of the area for seven different injection speeds for a fixed mobility ratio $R=1.03$. The area is measured as the area of the zone occupied by the glycerol sample in which the gray levels are larger than 0.83.

same viscosity than that of the displacing fluid, fingering does not occur, and two different regimes of dispersion and advective transport can be identified, depending on the injection speed. In this stable case, simple models of the temporal evolution of the sample length appeared to fit the experimental data reasonably well, moreover providing an estimate of the molecular diffusion coefficient and of the dispersion coefficient (although with a large error margin due to a strong sensitivity to the detection level of our optical system).

For an unstable viscous sample displaced by a less viscous miscible fluid, the rear interface can become unstable because of fingering phenomena. We have studied here experimentally the contribution of such fingering to the spreading of samples by analyzing the temporal evolution of the area and perimeter of samples of viscous aqueous/glycerol mixtures displaced in a Hele-Shaw cell by colored water. The

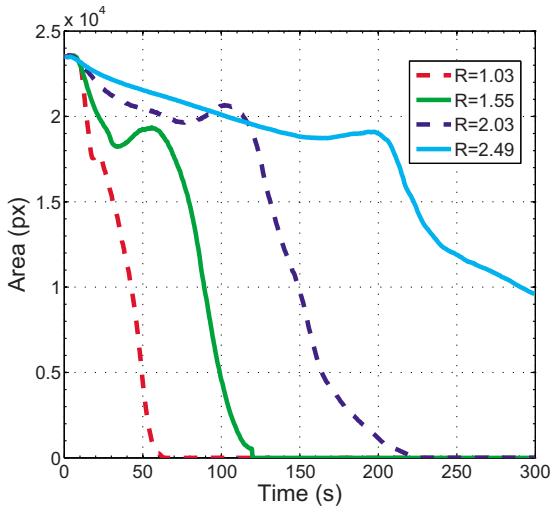

FIG. 18. (Color online) Temporal evolution of the area for four different mobility ratios and $U=7.50$ mm/s.

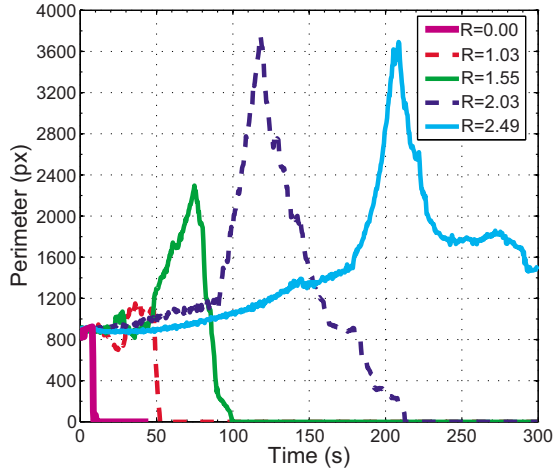

FIG. 19. (Color online) Temporal evolution of the perimeter for five different mobility ratios and $U=7.50$ mm/s.

larger the mobility ratio or the injection speed, the more complex the fingering pattern and the larger the distortion of the sample. Concerning the perimeter of an isoconcentration curve, its value is always larger for fingered samples than for stable ones. The maximum value of the perimeter reached before the sample starts to exit the cell does however not evolve monotonically with U. Indeed, at fixed R, this maximum value shows a minimum at an intermediate value of U, separating regimes of deformation in a few large fingers at small U and repeated splitting of numerous thin fingers at large U. At fixed speed but increasing R, the maximum value reached by the perimeter increases with R until saturating when the viscosity ratio is large enough to induce dislocation of the sample by the less viscous displacing fluid heading toward the sink. For what concerns the area of a given isoconcentration curve, the specificity of the geometry studied here, i.e., an initially circular sample drained out toward a point sink, leads to an overall decrease of the area. The development of fingering is witnessed by the presence on this temporal global decrease of bumps that contribute to an increase of the total area.

Our study shows that a Hele-Shaw cell is a good tool to understand and quantify the relative contribution of dispersion and fingering instabilities in the evolution of localized samples displaced by fluids with different viscosities as a function of the injection velocity. Even though there is an analogy between flows in Hele-Shaw cells and in porous media, allowing to expect that some of our observations could be transposed to applications such as contaminant spreading or chromatography, it remains to explore to what extent such analogy holds, in particular for real three-dimensional porous structures.

ACKNOWLEDGMENTS

The authors would like to thank J.-C. Dupin, L. Granger, C. Minetti, P. Queckers, L. Riand, and A. Vedernikov for help in the experiments and G.M. Homsy for fruitful discussions. R.M. has benefited from a FRIA Ph.D. fellowship.

G.R. and A.D. thank the IRSIB "Research in Brussels" program for support. A.D. thanks also ESA and BESLPO via the PRODEX Programme as well as FNRS and the Faculté des Sciences of ULB for support. P.C. gratefully acknowledges the financial support of the Fonds de la Recherche Scientifique (FNRS). The authors acknowledge the support from the Communauté Française de Belgique via the ARC Project No. 04/09-308 (ARCHIMEDES) and from the ITN-Marie Curie network MULTIFLOW.

[1] S. E. Serrano, "Propagation of nonlinear reactive contaminants in porous media," Water Resour. Res. **39**, 1228, doi:10.1029/2002WR001922 (2003).
[2] V. Kretz, P. Berest, J.-P. Hulin, and D. Salin, "An experimental study of the effects of density and viscosity contrasts on macrodispersion in porous media," Water Resour. Res. **39**, 1032, doi:10.1029/2001WR001244 (2003).
[3] A. De Wit, Y. Bertho, and M. Martin, "Viscous fingering of miscible slices," Phys. Fluids **17**, 054114 (2005).
[4] J. Bear, *Dynamics of Fluids in Porous Media* (Dover, New York, 1989).
[5] G. I. Taylor, "Dispersion of a soluble matter in solvent flowing slowly through a tube," Proc. R. Soc. London, Ser. A **219**, 186 (1953).
[6] R. Aris, "On the dispersion of a solute in a fluid flowing through a tube," Proc. R. Soc. London, Ser. A **235**, 67 (1956).
[7] R. Aris, "On the dispersion of a solute by diffusion, convection and exchange between phases," Proc. R. Soc. London, Ser. A **252**, 538 (1959).
[8] A. Boschan, V. J. Charette, S. Gabbanelli, I. Ippolito, and R. Chertcoff, "Tracer dispersion of non-Newtonian fluids in a Hele-Shaw cell," Physica A **327**, 49 (2003).
[9] J. Zhang and I. A. Frigaard, "Dispersion effects in the miscible displacement of two fluids in a duct of large aspect ratio," J. Fluid Mech. **549**, 225 (2006).
[10] M. L. Parks and L. A. Romero, "Taylor-Aris dispersion in high aspect ratio columns of nearly rectangular cross section," Math. Comput. Modell. **46**, 699 (2007).
[11] G. M. Homsy, "Viscous fingering in porous media," Annu. Rev. Fluid Mech. **19**, 271 (1987).
[12] C. Oltean, C. H. Felder, M. Panfilov, and M. A. Buès, "Transport with a very low density contrast in Hele-Shaw cell and porous medium: Evolution of the mixing zone," Transp. Porous Media **55**, 339 (2004).
[13] C. Oltean, F. Golfier, and M. A. Buès, "Experimental and numerical study of the validity of Hele-Shaw cell as analogue model for variable-density flow in homogeneous porous media," Adv. Water Resour. **31**, 82 (2008).
[14] C. Y. Jiao and H. Hötzl, "An experimental study of miscible displacements in porous media with variation of fluid density and viscosity," Transp. Porous Media **54**, 125 (2004).
[15] R. M. Smith, *Gas and Liquid Chromatography in Analytical Chemistry* (John Wiley & Sons, Chichester, 1988).
[16] G. Guiochon, A. Felinger, D. G. Shirazi, and A. M. Katti, *Fundamentals of Preparative and Nonlinear Chromatography* (Elsevier-Academic, San Diego, 2006).
[17] G. Rousseaux, A. De Wit, and M. Martin, "Viscous fingering in packed chromatographic columns: Linear stability analysis," J. Chromatogr. A **1149**, 254 (2007).
[18] M. Mishra, M. Martin, and A. De Wit, "Miscible viscous fingering with linear adsorption on the porous matrix," Phys. Fluids **19**, 073101 (2007).
[19] M. Mishra, M. Martin, and A. De Wit, "Differences in miscible viscous fingering of finite width slices with positive and negative log-mobility ratio," Phys. Rev. E **78**, 066306 (2008).
[20] M. Mishra, M. Martin, and A. De Wit, "Influence of miscible viscous fingering with negative log-mobility ratio on spreading of adsorbed analytes," Chem. Eng. Sci. **65**, 2392 (2010).
[21] T. T. Norton and E. J. Fernandez, "Viscous fingering in size exclusion chromatography: Insights from numerical simulation," Ind. Eng. Chem. Res. **35**, 2460 (1996).
[22] B. Broyles, R. Shalliker, D. Cherrak, and G. Guiochon, "Visualization of viscous fingering in chromatographic columns," J. Chromatogr. A **822**, 173 (1998).
[23] H. J. Catchpoole, R. A. Shalliker, G. Dennis, and G. Guiochon, "Visualising the onset of viscous fingering in chromatography columns," J. Chromatogr. A **1117**, 137 (2006).
[24] L. D. Plante, P. M. Romano, and E. J. Fernandez, "Viscous fingering in chromatography visualized via magnetic resonance imaging," Chem. Eng. Sci. **49**, 2229 (1994).
[25] M. L. Dickson, T. T. Norton, and E. J. Fernandez, "Chemical imaging of multicomponent viscous fingering in chromatography," AIChE J. **43**, 409 (1997).
[26] W. De Malsche, J. Op De Beeck, H. Gardeniers, and G. Desmet, "Visualization and quantification of the onset and the extent of viscous fingering in micro-pillar array columns," J. Chromatogr. A **1216**, 5511 (2009).
[27] C.-Y. Chen and S.-W. Wang, "Miscible displacement of a layer with finite width in porous media," Int. J. Numer. Methods Heat Fluid Flow **11**, 761 (2001).
[28] V. R. Dushin, V. F. Nikitin, Yu. G. Phylippov, and J.-C. Legros, Acta Astronaut. **66**, 742 (2010).
[29] Z. Pearl, M. Magaritz, and P. Bendel, "Nuclear magnetic resonance imaging of miscible fingering in porous media," Transp. Porous Media **12**, 107 (1993).
[30] F. Hoffman, D. Ronen, and Z. Pearl, "Evaluation of flow characteristics of a sand column using magnetic resonance imaging," J. Contam. Hydrol. **22**, 95 (1996).
[31] S. Oswald, W. Kinzelbach, A. Greiner, and G. Brix, "Observation of flow and transport processes in artificial porous media via magnetic resonance imaging in three dimensions," Geoderma **80**, 417 (1997).
[32] S. Hill, "Channeling in packed columns," Chem. Eng. Sci. **1**, 247 (1952).
[33] A. R. Kopf-Sill and G. M. Homsy, "Nonlinear unstable viscous fingers in Hele-Shaw flows. Part I: Experiments," Phys. Fluids **31**, 242 (1988).
[34] R. A. Wooding, "Instability of a viscous liquid of variable density in a vertical Hele-Shaw cell," J. Fluid Mech. **7**, 501 (1960).
[35] J. W. Elder, "Transient convection in a porous medium," J. Fluid Mech. **27**, 609 (1967).
[36] R. A. Wooding, S. W. Tyler, and I. White, "Convection in groundwater below an evaporating salt lake. 1. Onset of instability," Water Resour. Res. **33**, 1199, doi:10.1029/96WR03533 (1997).
[37] R. A. Wooding, S. W. Tyler, I. White, and P. A. Anderson, "Convection in groundwater below an evaporating salt lake. 2. Evolution of fingers or plumes," Water Resour. Res. **33**, 1219, doi:10.1029/96WR03534 (1997).
[38] A. Vedernikov, B. Scheid, E. Istasse, and J. C. Legros, "Viscous fingering in miscible liquids under microgravity conditions," Phys. Fluids **13**, S12 (2001).
[39] P. Petitjeans, C.-Y. Chen, E. Meiburg, and T. Maxworthy, "Miscible quarter-five spot displacements in a Hele-Shaw cell and the role of flow-induced dispersion," Phys. Fluids **11**, 1705 (1999).
[40] J. Crank, *The Mathematics of Diffusion* (Oxford University Press, Oxford, 1976).
[41] N. Rakotomalala, D. Salin, and P. Watzky, "Miscible displacement between two parallel plates: BGK lattice gas simulations," J. Fluid Mech. **338**, 277 (1997).
[42] C. Tan and G. Homsy, "Stability of miscible displacements in porous media: Rectilinear flow," Phys. Fluids **29**, 3549 (1986).